



Synthesis, Characterization, Optical, DFT, TD DFT Studies and *In silico* ADME Predictions of Thiosemicarbazone ligand and its Au(III) Complex

T. A. YOUSEF^{1,2*} and M. KHAIRY^{1,3}

¹Department of Chemistry, Science College, Imam Mohammad Ibn Saud Islamic University, (IMSIU), Riyadh, KSA, P.O. Box 90950, Riyadh 11623, Saudi Arabia

² Department of Toxic and Narcotic drug, Forensic Medicine, Mansoura Laboratory, Medicolegal organization, Ministry of Justice, Egypt

³ Chemistry department, Faculty of Science, Benha University, Benha, Egypt

*Corresponding author E-mail: tayousef@imamu.edu.sa

<http://dx.doi.org/10.13005/ojc/380303>

(Received: March 08, 2022; Accepted: May 13, 2022)

ABSTRACT

In the present work the reaction of hydrazone ligand with AuCl₃ was investigated. The ligand that could be obtained by the condensation of thiosemicarbazide with *p*-diaminobenzaldehyde belong to the class of mononegative or binegative bidentate ligands. The structure of the prepared samples has been defined by infrared spectroscopy, elemental analyzes, ¹H-¹³C NMR, SEM, and Powder XRD techniques. The ligand is present in both solid and liquid states in the thione form. The ligand is binding to Au via, azomethine nitrogen and thione sulfur atoms. Powder XRD pattern of ligand and [AuHLCI₂]Cl complex show several diffraction peaks with high intensity indicating the crystalline nature of them. The observation of new diffraction peaks at different positions indicates the successful formation of the complex. The synthesized ligand and complex have crystallites sizes of 103 and 46 nm, respectively indicating the nanostructure of them. The ligand and it complex shows different particles shapes of plates, sheets, and spheres. Optimizations of the geometries of the formed complex with gold and the ligand were carried out by using DFT in a gaseous state. The excited states of various multiplicities were examined by the TD-DFT.

Keywords: Gold complexes, Scanning Electron Microscopy, Powder XRD, DFT, TD-DFT.

INTRODUCTION

Thiosemicarbazones appear as ligands in complexes with transition metal ions. The formation of coordination bonds involves the sulfur and nitrogen atoms of hydrazine. Like thiosemicarbazones, metal complexes have also been extensively

studied for potential pharmacological activities. Their metal complexes are generally more active than free thiosemicarbazone. The coordination chemistry of nitrogen compounds is undergoing significant progress due to the diversity of the chemical and catalytic properties of complexes containing, in their coordination sphere, one or



more nitrogen functions¹⁻³. Thiosemicarbazones are of impressive intrigued because of their uses in pharmacological field, and their flexibility as ligands to create a wide assortment of modes of coordination⁴. Their importance as coordinating ligands is due to the presence of donor N and S atoms. Indeed, thiosemicarbazones signify to an expansive family of compounds with greatly different pharmacological properties, especially in the antimicrobial⁵, anticonvulsant⁶, antimalaria⁷, antiviral⁸, and especially antitumor⁹⁻¹². Gold(I) and gold(III) based complexes have demonstrated a wide range of biological features (anticancer, antiviral, and antiparasitic activity) and can be used as a substitute for cisplatin¹³. Apart from DNA, several peptides and enzymes have been identified as potential targets of gold(III) complexes^{14,15}. Gold complexes with an oxidation state of +1 or +3 have been utilized in the treatment of many diseases for decades, particularly rheumatoid arthritis¹⁶. They are ductile and malleable elements which have a very good corrosion resistance and therefore have found many applications through the ages. We resumed our previous reporting¹⁷ on HL coordination manners with the spectroscopic, optical band gap, ADMET and computational methods with Au(III).

EXPERIMENT

Materials and Physicochemical characterizations

The chemicals and solvents were purchased from Sigma-Aldrich and used as such in experiments. Elemental analyzes of nitrogen, hydrogen, carbon atoms were carried out by a GmbH VariuoEL V3.00 automatic elemental analyzer, IRIS ER/S•WP-1 ICP atomic emission spectrometer was used to evaluate the concentration of metals. VERTEX-70 FT-IR spectrophotometer was used to were measured the FT-IR spectra of samples mixed with KBr in the 400–4000 cm^{-1} margin. UV–Vis absorptions spectra of prepared materials were measured using the Shimadzu UV–2550 spectrometer and 970 CRT spectrofluorometer (Spectro Shanghai) in DMSO solution. ¹H-¹³CNMR spectra of the ligand were carried out with a Mercury Plus (400 MHz) spectrometer in D₂O-DMSO solution, and the chemical shifts determined in ppm relatives to the internal TMS (H). Agilent SuperNova Dual area detector diffractometer was used to measure the X-ray diffraction patterns of the complexes. SEM was used to investigate the powder's morphology

(JSM-6380LA, JEOL-Japan Electron Optics Laboratory, Tokyo, Japan).

Synthesis of ligand

The ligand was prepared as previously described¹³.

Synthesis of gold complex [AuHLCI₂]Cl

The gold complexes were produced by mixing a 1:1 ligand-to-metal molar ratio ethanolic solution of the thiosemicarbazone ligand (1 mmol) with (HAuCl₄•3H₂O) at room temperature with stirring for 2 hours. The particles were then filtered out, washed in acetone, and dried under vacuum.

Yield 71%; colour golden yellow, elemental anal. Calc. for C₁₀H₁₄AuCl₃N₂S (525.63) calculated: C 22.85, H 2.68, N 10.66, Cl 20.23, S 6.54. Found C 22.76, H 2.73, N 11.09, Cl 20.78, S 6.21. FT-IR (KBr, cm^{-1}): 3375 $\nu(\text{NH}_2)$, 3228 $\nu(\text{NH})$, 1599 $\nu(\text{C}=\text{N})$, 1180 and 790 $\nu(\text{C}=\text{S})$, 945 $\nu(\text{N}-\text{N})$, 430 $\nu(\text{Au}-\text{S})$, 372 $\nu(\text{Au}-\text{N})$. UV-Vis (λ_{max} , nm, DMSO): 255, 345, 465, Mol. Cond. (DMF, $\Omega^{-1}\text{cm}^{-1}\text{mol}^{-1}$): Ωm 78.

Molecular modeling

The optimization of the molecular structure of the composition is calculated from the functional hybrid B₃LYP^{18,19} which is the functionally correlation of Lee- Yang-Parr associated with a functional hybrid exchange proposed by Becke and 6-31G (d, p), implemented in Gaussian 09²⁰. The Gauss View 5 program was used to visualize the theoretical data obtained²¹, the HOMO and LUMO energies were calculated using the DFT method from state geometry fundamentals of the molecule taken to the gaseous state as well as in different solvents such as that water and ethanol. Atomic charges were also present were studied at the average B₃LYP/6-31G (d, p) level of the DFT. Two essential steps are necessary to obtain the absorption wavelengths. The first step consists in optimizing the ground state of each molecule at the level of the restricted spin, without symmetry constraint, by performing standard DFT calculations using the B3PW91 functional, associated with the augmented LANL2DZ base for Au with polarization functions on all atoms, except for hydrogen²²⁻²⁴. In the second step, TD-DFT is implemented to determine the absorption wavelengths of all the molecules studied, ten excited states having been calculated in this work.

RESULTS AND DISCUSSION

The ligand and its Au complex were synthesized by precipitation reactions and characterized by analytical methods and spectroscopic techniques. Au complex is non-electrolyte, suggesting that the chlorides are inside the coordination sphere. The elementary analyzes show a good harmony between the values found and calculated corresponding to the proposed structure.

Spectroscopic characterization

The ^1H - ^{13}C NMR spectra of HL in DMSO- d_6 (Figs.1,2) were recorded. With D_2O , the NH protons disappeared, indicating that they can be easily replaced. The IR spectra of the coordination compounds and the ligand were related to each other to compare. The significant differences in the displacement of the IR bands indicate the coordination modes. The ligand can coordinate as a neutral ligand in the thione form. This mode can be based on the shifts in the corresponding bands in comparison to the uncoordinated ligand can be demonstrated.

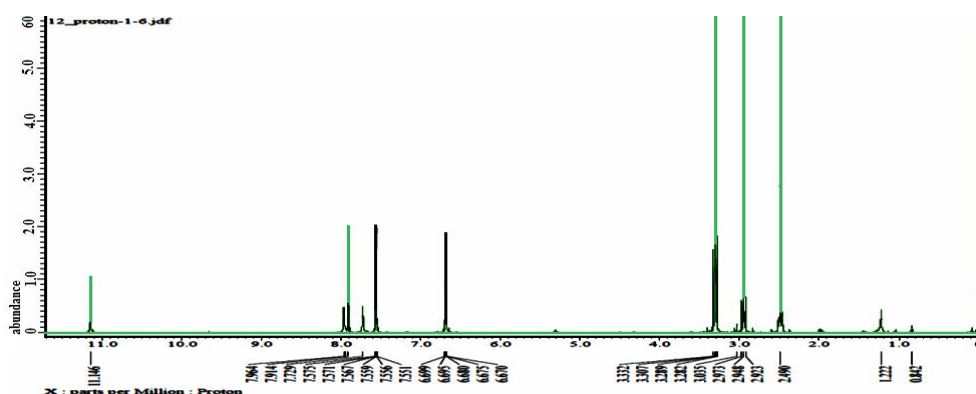


Fig. 1. ^1H NMR spectrum of HL

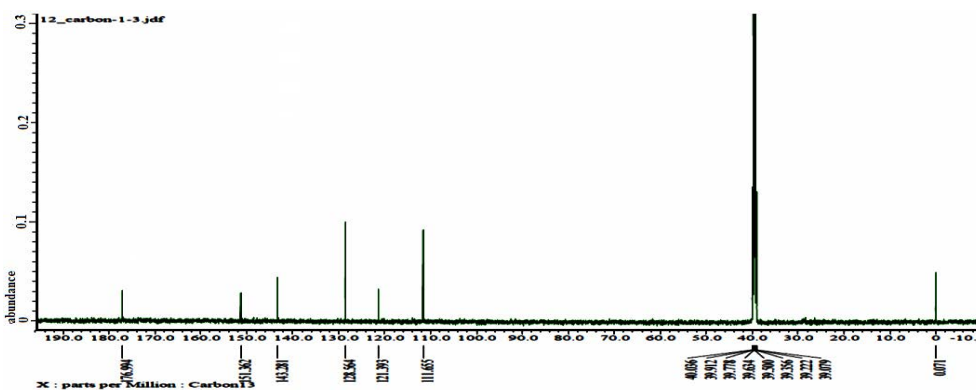


Fig. 2. ^{13}C NMR spectrum of HL

The ligand's IR spectra lacks the $\nu(\text{S-H})$ band, which is normally situated about 2570 cm^{-1} . The (NH) band, on the other hand, may be found at 3243 cm^{-1} . The ligand is thus within thione form within the solid state. This confirmed via the observation of the $\nu(\text{C}=\text{S})$ band at 812 and 1165 cm^{-1} ^{17, 25}.

In $[\text{AuHLCl}_2]\text{Cl}$ complex in which the nitrogen atom of the groups of imine and the sulfur atom of the groups of thione are linked to the Au (III) ion. This mode of complexation is verified through:

1. The decreased of the azomethine's $\nu(\text{C}=\text{N})$

vibration in the complexes designates that the nitrogen of azomethine is shared in the coordination.

2. $\nu(\text{C}=\text{S})$ band has decreased by 22 cm^{-1} .
3. Appearance of new bands attributable to $\nu(\text{M}-\text{N})$, and $\nu(\text{M}-\text{S})$, at 430 and 372 cm^{-1} respectively.
4. Shift of $\nu(\text{N}-\text{N})$ band to higher wavenumber.

Electronic spectra

Electronic spectra for the ligand and its $[\text{AuHLCl}_2]\text{Cl}$ complex were shown in a

dimethylsulfoxide (DMSO) solution. The ligand's electronic spectrum revealed three strong bands at 282, 307, and 350nm indicating $\pi \rightarrow \pi^*$ and $\sigma \rightarrow \sigma^*$ transitions. The electronic spectra of Au(III) complex showed bands at 255, 345, and 465nm which may be assigned to $^1A_{1g} \rightarrow ^1B_{1g}$, $^1A_{1g} \rightarrow ^1E_{1g}$ and $^1A_{1g} \rightarrow ^1A_{2g}$ respectively. A charge transfer transition occurs around 345nm. As a result, the Au(III) complex might have a square planar geometry²⁶.

Molecular modeling

Bond length and bond angles measurements

DFT has shown to be a potent, high-precision method for reproducing experimental values of frequencies of vibration, geometry of molecules, polar moments, atomic charges, and thermodynamic characteristics, among other things.²⁷⁻²⁹

Optimizations of the geometries of the complex with gold and ligand were approved via using DFT, the structures are represented in Figs. 3 and 4, with the numbering of atoms. The main geometric parameters of the complex with gold and ligand are given in Table 1 where the lengths of bonds are represented in angstroms and the angles in degrees.

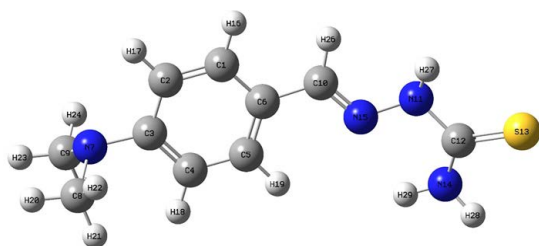


Fig. 3. Optimized molecular structure of HL

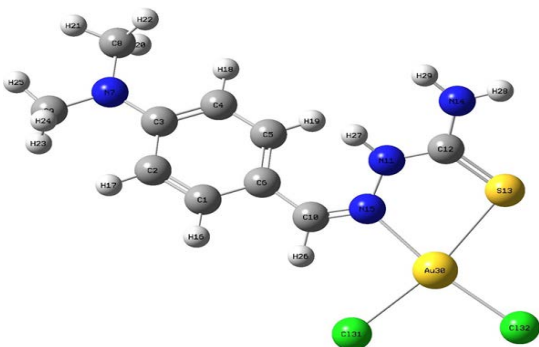


Fig. 4. Optimized molecular structure of [AuHLCI₂]Cl complex

The first observation on the molecular structure obtained is that the complex adopts a

square planar geometry, with the ligand bound in a bidentate manner through the nitrogen and sulphur atoms, the coordination sphere being completed by two chlorine atoms. Not having experimental values on the geometric parameters (X-ray single crystal experimental technique could not be performed for the complex), we therefore compared our values with the results found in the study of ligand.

It can be seen, on reading the results given in Table 1, that the lengths of the different bonds such as C(12)-S(13), N(11)-N(15) and C(10)-N(15) of the [AuHLCI₂]Cl complex are slightly greater than those obtained in the uncoordinated ligand because of the presence of the metal ion bound to the ligand^{17,30}. As has been observed with the ligand, the Au(III) complex formed with the ligand are in the plane.

Table 1: Main geometric parameters of ligand and its Au(III) complex distances are in angstroms (Å) and angles in degrees (°).

H ₂ L		[AuHLCI ₂]Cl	
Bond	Length(Å)	Bond	Length(Å)
C(12)-S(13)	1.65	C(12)-S(13)	1.74
C(12)-N(14)	1.38	C(12)-N(14)	1.37
C(12)-N(11)	1.43	C(12)-N(11)	1.37
N(11)-N(15)	1.39	N(11)-N(15)	1.45
C(10)-N(15)	1.30	C(10)-N(15)	1.41
C(10)-C(6)	1.46	C(10)-C(6)	1.46
C(3)-N(7)	1.47	C(3)-N(7)	1.38
Angle	Degree(°)	Angle	Degree(°)
S(13)-C(12)-N(14)	123.32	S(13)-C(12)-N(14)	120.16
N(11)-C(12)-N(14)	116.04	N(11)-C(12)-N(14)	115.37
C(12)-N(11)-N(15)	117.38	C(12)-N(11)-N(15)	122.30
C(10)-N(15)-N(11)	120.60	C(10)-N(15)-N(11)	119.42
C(6)-C(10)-N(15)	120.38	C(6)-C(10)-N(15)	130.53
C(5)-C(6)-C(10)	122.63	C(5)-C(6)-C(10)	125.63

Mulliken charge

The analysis of the Mulliken net atomic charges, given in Table 2, shows that the negative charge of the nitrogen of the azomethine group and S of thione group are the greatest negative charge in comparison with other atoms of ligand. This result suggests that the nitrogen atom azomethine group and S atom of thione group are reactive sites for metal attack, thereby leading to coordination of ligand to metal ions through nitrogen and sulphur which agree with experimental results.

Table 2: Net Mulliken charges of the atoms for the ligand in the ground state in the gas phase an

Atom	Charge
C 1	-0.35
C 2	-0.05
C 3	-0.87
C 4	-0.52
C 5	-0.15
C 6	1.19
N 7	0.26
C 8	-0.25
C 9	-0.26
C 10	0.81
N 11	0.06
C 12	-0.03
S 13	-0.41
N 14	-0.27
N 15	-0.80

TD DFT studies

In UV-Visible absorption, fluorescence and phosphorescence spectroscopy, molecular orbitals (MO) are used to describe the fundamental state and the excitation state of a molecule. High-energy molecular orbitals are called HOMOs and unoccupied molecular orbitals of low-energy are called LUMOs.

The molecule, in the resting state, has the property to absorb the energy emitted by a luminous

source in the form of a photon and obtain a higher energy level; such a transition corresponds to the promotion of an electron into an orbit free of higher energy. The molecule is said to be excited by energy gain^{31,32}. The absorption of an appropriate energy photon (UV-Visible domain) causes a molecule from the fundamental state to pass into an excited electronic state; the UV-Visible absorption bands of the molecules are characterized by a maximum absorption wavelength (λ_{max}).

The geometries of the complex with gold and ligand were completely optimized, without symmetry constraint in the first excited state S1 using the TDDFT method with the B3PW91 functional and the LanI2dz base.

TDDFT calculations demonstrate that the ligand's UV-Visible spectra have 3 major peaks that are extremely similar to observed peaks, the peak at 282nm is due to HOMO-1 \longrightarrow LUMO, 307nm correspond to HOMO-2 \longrightarrow LUMO and 350nm correspond to HOMO \longrightarrow LUMO transition. In case of [AuHLCI₂]₂Cl complex the peak at 255nm is due to HOMO-2 \longrightarrow LUMO, 345nm correspond to HOMO-1 \longrightarrow HOMO and 465nm correspond to HOMO \longrightarrow HOMO transition Table 3.

Table 3: Calculated and experimental absorption wavelengths, data in nanometers (electronvolt), and oscillator force (f) of ligand and its Au(III) complex

λ exp max nm (eV)	H ₂ L		f	[AuHLCI ₂] ₂ Cl		f
	λ cal max nm (eV)			λ exp max nm (eV)	λ cal maxnm (eV)	
350	358 (3.463)		0.057	465	445 (2.786)	0.004
307	314 (3.949)		0.004	345	410 (3.024)	0
282	296 (4.189)		0.504	255	286 (4.335)	0

Table 4: *In silico* ADME predictions physiochemical properties of synthesized compounds

	H ₂ L	[AuHLCI ₂] ₂ Cl
Molecular weight	222.31 g/mol	490.18 g/mol
Num. heavy atoms	15	18
Num. arom. heavy atoms	6	6
Fraction Csp3	0.20	0.20
Num. rotatable bonds	4	2
Num. H-bond acceptors	1	0
Num. H-bond donors	2	2
Molar Refractivity	67.41	96.35
TPSA	85.74 Å ²	85.74 Å ²

TPSA: Topological polar surface area

XRD analysis

Due to the difficulty of synthesis single crystal of gold complex with ligand containing sulphur and nitrogen as donor atoms which can form a polymeric state by the intramolecular interactions^{33, 34}. Thus, powder X-ray diffraction analysis was measured to identify its phase structure, crystallinity, and the purity of samples.

XRD was used to determine whether the generated samples were polycrystalline or amorphous. Powder XRD pattern of H₂L and [AuHLCI₂]₂Cl complex were carried out over the 2θ (scattering angle) = 10–80° range and represented in Fig. 5a. It was observed that the XRD pattern of ligand shows several diffraction peaks with main peak at 2θ=22.82°. The pattern exhibited sharp crystalline peaks indicating the high crystallinity (Fig. 5b). On the other hand, The XRD pattern of [AuHLCI₂]₂Cl complex shows completely different peaks observed at 2θ at 37.37°, 43.58°, 63.91°, 76.97° and 81.2°, respectively. The Shift observed in XRD peaks

especially for the main peak from 22.82° of ligand to 37.37° of complex was indicating the change of phase structure and the successful formation of complex through chelation of Au(III) with HL.

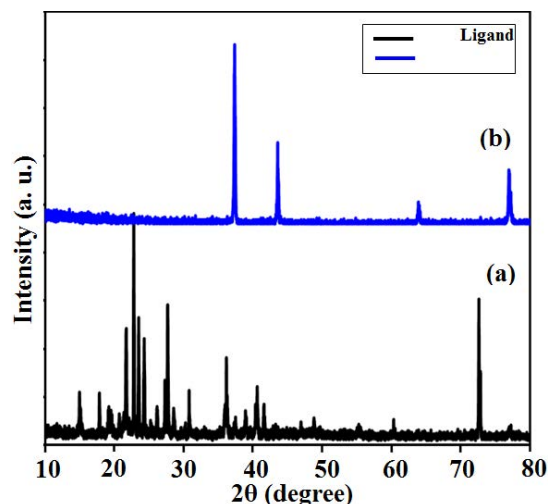


Fig. 5. XRD patterns of a) ligand and b) [AuHLCI₂]₂Cl complex

Table 5: *In silico* ADME predictions lipophilicity and water solubility of synthesized compounds

	H ₂ L	[AuHLCI ₂] ₂ Cl
Log Po/w (iLOGP)	2.04	0.00
Log Po/w (XLOGP3)	0.79	3.63
Log Po/w (WLOGP)	0.92	1.53
Log Po/w (MLOGP)	1.14	1.32
Log Po/w (SILICOS-IT)	1.62	-0.95
Consensus Log Po/w	1.30	1.11
Log S (ESOL)	-1.75	-5.28
Solubility	3.97e+00 mg/ml; 1.79e-02 mol/l	2.57e-03 mg/ml; 5.24e-06 mol/l
Class	Very soluble	Moderately soluble
Log S (Ali)	-2.17	-5.12
Solubility	1.50e+00 mg/ml; 6.74e-03 mol/l	3.73e-03 mg/ml; 7.61e-06 mol/l
Class	Soluble	Moderately soluble
Log S (SILICOS-IT)	-2.45	-4.42
Solubility	7.82e-01 mg/ml; 3.52e-03 mol/l	1.88e-02 mg/ml; 3.83e-05 mol/l
Class	Soluble	Moderately soluble

The average size of crystals (D_{XRD}) of the crystalline complexes was estimated via line broadening of the main peaks through the Scherrer's relation.³⁵

$$D_{XRD} = 0.9 k / \beta \cos \theta$$

Where k is the Ni K radiation's X-ray wavelength ($k = 0.154\text{nm}$), is Bragg's angle, and β is the whole width of the diffraction peak at half of its greatest intensity. It was found that, the crystal

sizes of ligand and [AuHLCI₂]₂Cl complex are 103 and 46nm. This is indicating the high crystallinity of synthesized ligand and the successful synthesis of nano-complex within nano-sized range.

The high crystallinity and the diffraction peaks observed in ligand may be attributed to the stacking structure of the layered structure due to the intermolecular π - π ^{36,37}. The slightly low crystallinity (46nm) and decreasing of diffraction intensity of

the $[\text{AuHLCI}_2]\text{Cl}$ complex compared to the ligand can be ascribed to metal ion coordination and counter anions doping which may weakened the intermolecular π - π stacking³⁸.

SEM Analysis

The shape, organization, and degree of aggregation of nanoparticles were all studied using SEM. The SEM micrographs (morphology) of the H_2L and $[\text{AuHLCI}_2]\text{Cl}$ complex have been taken in different magnification and given in Fig. 6. The SEM images of ligand (H_2L) (Fig. 6a, b, c) showed clusters of particles in the form of large rectangular plates on the micrometer scale and showed merged nanosheets (Fig. 6a). On the other hand, the morphology of complex has some changes in the shape of particles (Fig. 6d, e, f). The SEM image of complex showed different particles spherical and sheet like shapes. From these results we can conclude the modification

of the complex structure compared to the structure of ligand indicates the formation of complex.

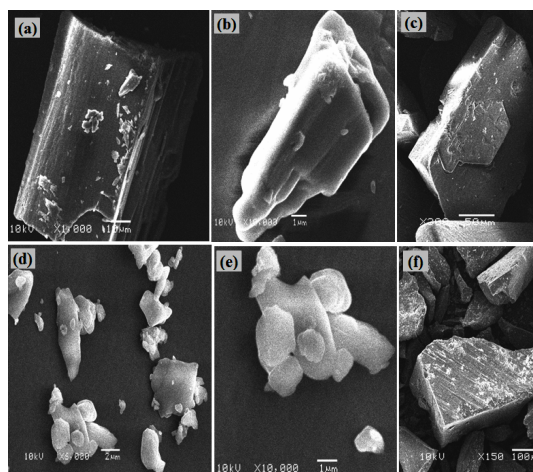


Fig. 6. SEM images of ligand (a, b, c) and $[\text{AuHLCI}_2]\text{Cl}$ complex (d, e, f) with different magnifications

Table 6: *In silico* ADME predictions pharmacokinetics and druglikeness of synthesized compounds

	H_2L	$[\text{AuHLCI}_2]\text{Cl}$
GI absorption	High	High
BBB permeant	No	No
P-gp substrate	No	No
CYP1A2 inhibitor	Yes	Yes
CYP2C19 inhibitor	No	Yes
CYP2C9 inhibitor	No	No
CYP2D6 inhibitor	No	No
CYP3A4 inhibitor	No	Yes
Log Kp (skin permeation)	-7.10 cm/s	-6.71 cm/s
Lipinski	Yes; 0 violation	Yes; 0 violation
Ghose	Yes	No; 1 violation: MW>480
Veber	Yes	Yes
Egan	Yes	Yes
Muegge	Yes	Yes
Bioavailability Score	0.55	0.55

Optical band gap calculation

The optical absorption spectrum is one of the most important methods used to calculate the energy gap. Electrons are excited from the HOMO to LUMO as a result of light absorption with an appropriate energy higher than the difference between the two orbitals. This process gives important information about the nature and value of the band gap.

The optical band gap (E_g) of ligand and Au complex was determined using the Tauc equation^{39,40}:

$$\alpha hv = k (hv - E_g)^n \tag{1}$$

Where α is the coefficient of absorption, k is constant, and E_g is the material's optical band gap and The exponent n primarily based totally at the kind of the electronic transition; for transitions that direct allowed and not allowed $n = 1/2$ and $3/2$, respectively, for transitions that indirect allowed and not allowed $n = 2$ and 3 , respectively. The values of energy gap were determined from the relationship (1) via plot $(\alpha hv)^2$ vs. hv as shown in Fig. 7, intersection of the straight line of the curve at $(\alpha hv)^2 = 0$, a direct band gap was discovered.

It was found the n exponent equal $1/2$ indicating the direct transition (allowed). The E_g -values of ligand and $[\text{AuHLCI}_2]\text{Cl}$ complex

were found experimentally to be 3.32 eV and 2.44 eV, respectively. The results show the energy gap of complex is lower than the gap of the ligand, demonstrating that (E_g) decrease upon complexation with metal ions. This suggest that the $[\text{AuHLCI}_2]\text{Cl}$ complex is semiconductor and as shown by the band gap values, fall within the same region of highly effective solar

materials. As a result, the current materials could be evaluated as interested materials for applications of solar cell that gather solar energy from the home⁴¹. On the other hand, the theoretical band gap was found to be 3.36 eV and 2.46 eV for ligand and $[\text{AuHLCI}_2]\text{Cl}$ complex, respectively. These values in good matching with the experimental values.

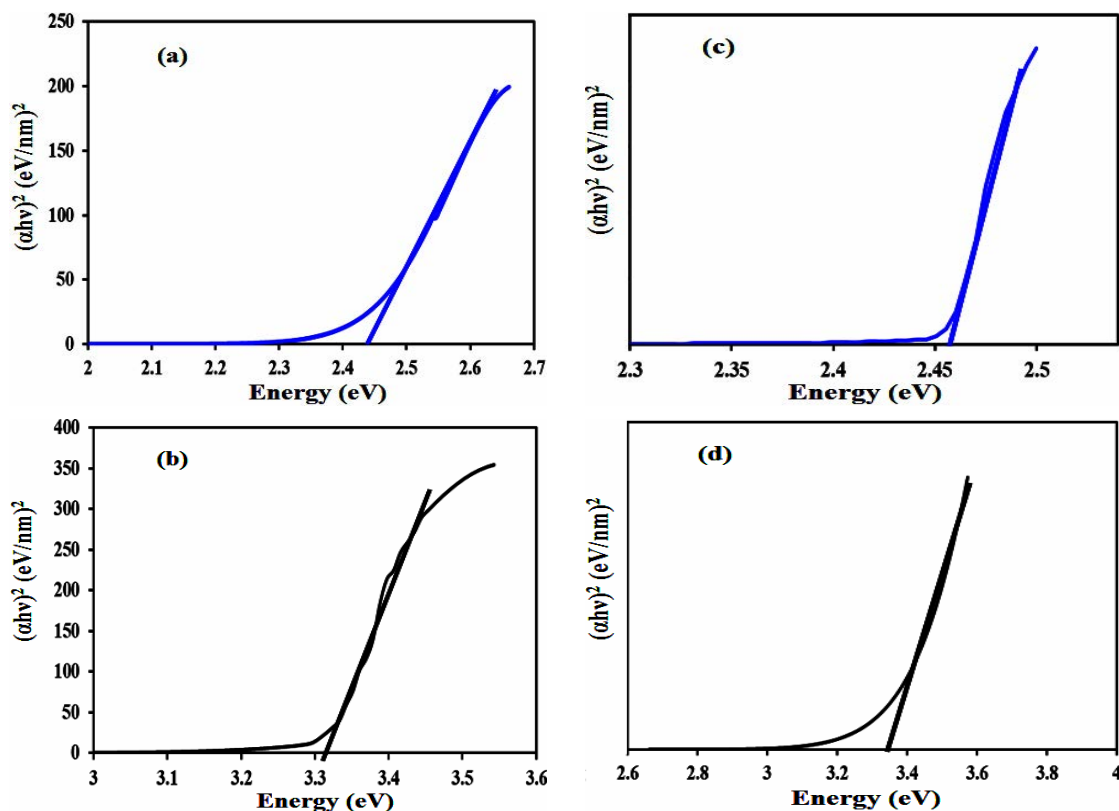


Fig. 7. Band gap curves of a) ligand, b) $[\text{AuHLCI}_2]\text{Cl}$ complex experimentally and band gap curves of c) ligand and d) $[\text{AuHLCI}_2]\text{Cl}$ theoretically

***In silico* ADME predictions**

Using the Swiss ADME web tool, an *in silico* ADME (Absorption, Distribution, Metabolism, and Excretion) research of ligand and its Au(III) complex were done, and essential physiochemical parameters were estimated^{42,43}. Tables 4-6 show the values of Physiochemical properties, lipophilicity, water solubility, Pharmacokinetics and Drug likeness of ligand and its Au(III) complex. Both of The complex with gold and the ligand exhibit good membrane permeability (BBB) with high gastrointestinal absorption GI. The complex with gold and the ligand pharmacophore or

drug-like characteristics revealed that they all follow and satisfy the Lipinski rule, with all of their attributes falling within a tolerable range. Furthermore, as shown in Fig. 8, the ligand and its Au(III) complex oral bioavailability radar chart revealed their projected oral bioavailability as well as their favorable pharmacokinetic. Also, features the Radar plot displays a zone with the optimal range of drug likeness, with the exception of a minor polarity deviation⁴⁴. The compounds that met the conditions of Lipinski's rule of five with zero violation in this *in silico* ADME prediction had the potential to evolve into a good oral drug candidate.

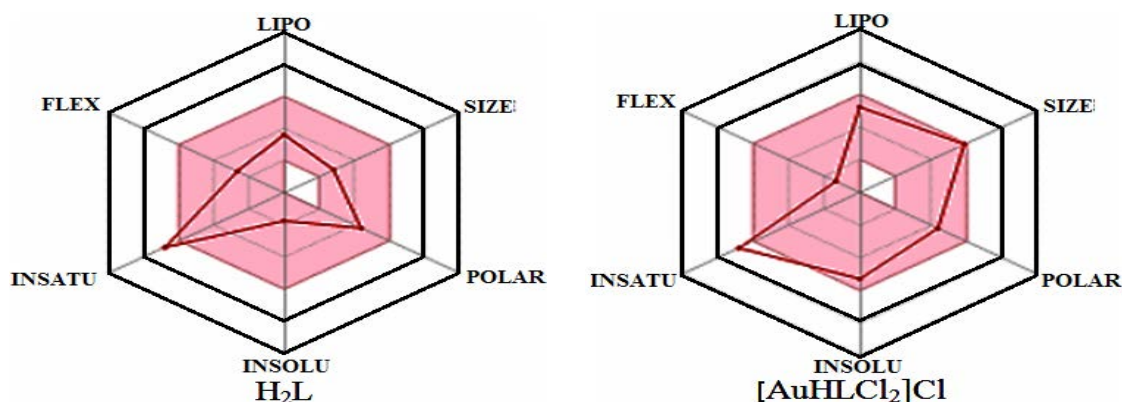


Fig. 8. bioavailability radar chart of ligand and its Au(III) complex [Pink area in plotted graph represents a favorable set of properties for excellent oral bioavailability. LIPO (Lipophilicity), XLOGP between -0.7 and $+5.0$, SIZE (Molecular weight and range = 150 to 500 g/mol), POLAR (Polarity), TPS (20 and 130 Å²), INSOLU (Solubility), LogS not higher than 6, INSATU (Saturation), FLEX (Flexibility), and no more than 8 rot able bond]

CONCLUSION

The bibliographic analysis of the work carried out on thiosemicarbazone and its gold complex have shown that the behavior of functional groups with respect to gold chloride. $[\text{AuHLCI}_2]\text{Cl}$ complex has square planner geometry. The bonding of the ligand and Au(III) occurs through nitrogen atoms of azomethine and sulfur atoms of thione. XRD reveals the high crystallinity of synthesized ligand and the efficacious synthesizing of nano-complex in nano-sized range. The SEM image of complex showed different particles spherical and sheet like shapes. The theoretical band gap was found to be 3.36 eV and 2.46 eV for ligand and $[\text{AuHLCI}_2]\text{Cl}$ complex, respectively. These values

in good matching with the experimental values. Excellent agreement between DFT studies and Experimental results. Finally, the in silico ADME results show that the materials follow Lipinski's rule of 5 with zero violations and have good oral bioavailability.

ACKNOWLEDGEMENT

This research was supported by the Deanship of Scientific Research, Imam Mohammad Ibn Saud Islamic University, Saudi Arabia, Grant No. (19-12-12-012).

Conflict of interest statement

The authors declare no conflict of interest.

REFERENCES

- Ghosh, M.; Biswas, P.; flörke, U.; Nag, K. *Inorg. Chem.*, **2008**, *47*, 281-296.
- Cui, X.; Zhou, Y.; Wang, N.; Liu, L.; Guo, Q.-X. *Tetrahedron Lett.*, **2007**, *48*, 163-167.
- Stephen J. S.; Haiwen Z.; Paul A.C.; Ciara P.M.; Eric J.D.; Christopher M.V.; Mazen T.S.; Andreas D.; Stephen A.W. *Polyhedron.*, **2004**, *23*, 2169-2176.
- Rômulo P. B.; Rafaelde L. P.; Edovando J. F. R.; Alexandra de S. F.; Leandro B.; Vanessa C.; Félix A. A. S.; Nilda V. B. *Life Sci.*, **2011**, *89*, 20-28.
- Ahmed E.; Mahmoud B. I. M.; Ammar M. M.; Rabie S. F.; Abdou. S. El-T.; Ahmed R. *J. Mol. Struct.*, **2022**, *1251*, 132004.
- Eman A. F.; Ahmed R.; Rogy R. E. E.; Ashraf H. B.; Yousry A. A. *Bioorg. Chem.*, **2021**, *116*, 105300.
- Jia-Qi L.; Han G.; Le Z.; Le-Yun S.; Cheng C.; Jia-Zhu C.; Huan-Huan D.; Ke-Wu Y. *Bioorg. Medic. Chem.*, **2021**, *38*, 116128.
- Wahid M. B.; Samir Y. A.; Khairy A. M.El-B.; Reham M. D.; Mostafa K.E. *Synth. Communic.*, **2021**, *51*, 2168-2174.
- Gabrieli L. P.; Raquel G. d. S., Heloisa B. *Coord. Chem. Rev.*, **2022**, *458*, 214418.
- Anna M.-W.; Katarzyna M.; Marta R.; Jaroslaw P.; Robert M. *Eur. J. Med. Chem.*, **2019**, *171*, 180-194.
- Balakrishnan N.; Haribabu J.; Eshaghi M. R.; Swaminathan S.; Balachandran C.; Bhuvanesh N.; Aoki S.; Karvembu R. *Inorg. Chim. Acta.*, **2022**, *534*, 120805.

12. Ozlem A.; Anita M. G.; Christina N. B.; Sotiris K. H.; Maciej K.; Ibrahim I. O. *Polyhedron.*, **2022**, *215*, 115683.
13. Magdalena M.; Dariusz C. B.; Urszula K. K.; Agnieszka K.; Magdalena D.; Anna ´S.; Edyta D-K.; Wiktoria J. *J. Inorg. Biochem.*, **2021**, *215*, 111311.
14. Porchia M.; Pellei M.; Marinelli M.; Tisato F.; Del B. F.; Santini C. *Eur. J. Med. Chem.*, **2018**, *146*, 709-746.
15. Mora M.; Gimeno M.C.; Visbal R. *Soc. Rev.*, **2019**, *48*, 447-462.
16. Radisavljević S.; Petrović B. *Front. Chem.*, **2020**, *8*, 1-8.
17. Yousef T. A. *Biointerface Res. Appl. Chem.*, **2019**, *9*, 4567-4574.
18. Lee C.; Yang W.; Parr R.G. *Phys. Rev. B.*, **1988**, *37*, 785-789.
19. Becke A.D. *J. Chem. Phys.*, **1993**, *98*, 5648-5652.
20. Frisch M.J.; Trucks G.W.; Schlegel H.B.; Scuseria G.E.; Robb M.A.; Cheeseman J.R.; Scalmani G.; Barone V.; Mennucci B.; Petersson G.A.; Nakatsuji H.; Caricato M.; Li X.; Hratchian H.P.; Izmaylov A.F.; Bloino J.; Zheng G.; Sonnenberg J.L.; Hada M.; Ehara M.; Toyota K.; Fukuda R.; Hasegawa J.; Ishida M.; Nakajima T.; Honda Y.; Kitao O.; Nakai H.; Vreven T.; Montgomery Jr. J.A.; Peralta J.E.; Ogliaro F.; Bearpark M.; Heyd J.J.; Brothers E.; Kudin K.N.; Staroverov V.N.; Kobayashi R.; Normand J.; Raghavachari K.; Rendell A.; Burant J.C.; Iyengar S.S.; Tomasi J.; Cossi M.; Rega N.; Millam J.M.; Klene M.; Knox J.E.; Cross J.B.; Bakken V.; Adamo C.; Jaramillo J.; Gomperts R.; Stratmann R.E.; Yazyev O.; Austin A.J.; Cammi R.; Pomelli C.; Ochterski J.W.; Martin R.L.; Morokuma K.; Zakrzewski V.G.; Voth G.A.; Salvador P.; Dannenberg J.J.; Dapprich S.; Daniels A.D.; Farkas O.; Foresman J.B.; Ortiz J.V.; Cioslowski J.; Fox D.J.; Gaussian 09, revision A.1, Gaussian, Inc, Wallingford., **2009**.
21. Dennington R.; Keith T.; Millam J.; Gauss View Version 5," Semichem Inc., Shawnee Mission., **2009**.
22. Kohn W., Sham L. *J. Phys. Rev. J. Phys. Rev.*, **1965**, *140*, A1133-1138.
23. Perdew J. P. *Phys. Rev. B* **1986**, *33*, 8822-8824.
24. Perdew J.P.; Burke K.; Wang Y. *Phys. Rev. B.*, **1996**, *54*, 16533-16539.
25. Yousef T.A.; Abu El-Reash G.M.; El-Rakhawy E.R. *Spectrochim. Acta Part A* **2014**, *133*, 568-578.
26. Mason W. R. I.; Gray H. B. *Inorg. Chem.*, **1968**, *7*, 55-58.
27. Saad S.; Hela F.; Ismail A.; Tarek Y. *J. Mol. Struct.*, **2021**, *1245*, 131072.
28. Temel E.; Alasalvar C.; Gokce H.; Guder A.; Albayrak C.; Alpaslan Y. B.; Alpaslan G.; Dilek N. *Spectrochim. Acta A* **2015**, *136*, 534-546.
29. Ceylan U.; Tarı G. O.; Gokce H.; Ağar E. *J. Mol. Struct.*, **2016**, *1110*, 1-10.
30. Yousef T.A. *J. Mol. Struct.*, **2020**, *1215*, 128180.
31. Yang W. T.; Mortier W. J. *J. Am. Chem. Soc.*, **1986**, *108*, 5708-5711.
32. Valeur B., *Molecular fluorescence.*, **2002**, *14*, 447-531.
33. Altaf M.; Helen S.-E.; Alexandre C.; Daisy N. S.; Fernando R. P.; Clarice Q. F. L.; Saeed A.; Mohammed B.; Mostafa M.; Fatima Z. K.; Taibi B. H. *Polyhedron.*, **2013**, *62*, 138-147.
34. Nomiya K.; Takahashi S.; Noguchi R. *J. Chem. Soc., Dalton Trans.*, **2000**, *13*, 2091-2097.
35. Samah S. S.; Wafaa A. B.; Mohamed K.; Mahmoud A. M. *Biointerface Res. Appl. Chem.*, **2022**, *12*, 1335-1350.
36. Li L. ; Lu F. ; Xue R. ; Ma B. ; Li Q. ; Wu N. ; Liu H. ; Yao W. ; Guo H. ; Yang W. *ACS Appl. Mater. Interfaces.*, **2019**, *11*, 26355.
37. Bhanja P.; Bhunia K.; Das S. K.; Pradhan D.; Kimura R.; Hijikata Y.; Irle S.; Bhaumik A. *Chem Sus Chem.*, **2017**, *10*, 921-928.
38. Xuedong M.; Qian L.; Yaoyao Z.; Wei W.; Yingmin G.; Cunshe Z. *J. Electrochem. Soc.*, **2020**, *167*, 090544.
39. Mott N.F.; Davis E.A. Calendron Press, Oxford., **1979**.
40. Khairy M.; Gouda M. E. *J. Adv. Res.*, **2015**, *6*, 555-562.
41. Fu M. L.; Guo G. C.; Liu X.; Cai L. Z.; Huang J. S. *Inorg. Chem. Commun.*, **2005**, *8*, 18-21.
42. Jatczak M.; Muylaert K.; De Coen L.M.; Keemink J.; Wuy B.; Augusti-Jins P.; Stevens C.V. *Bioorg. Med. Chem.*, **2014**, *22*, 3947-3956.
43. Arif R.; Rana M.; Yasmeen S.; Khan M.S.; Abid M.; Khan M.S.; Rahisuddin. *J. Mol. Struct.*, **2020**, *1208*, 127905.
44. Nesreen T. E.; Ahmed M. A.; Rageh K. H.; Moez A. I.; Abdulrahman G. A.; Mortaga M. A. *Molecules.*, **2022**, *27*, 620-637.